Iranian Journal of Chemistry and Chemical Engineering (IJCCE)

Wastewater treatment by new high-performance activated carbon from Semecarpus Anacardium and Quercus Infectoria nutshells: applications- kinetic and equilibrium studies

Naser Ghasemzadeh[a], Mohammad Ghadiri[b,*], Alireza Behroozsarand[a], Mehrdad Seifali Abbas Abadi[c,d]

[a] *Department of Chemical Engineering, Faculty of Renewable Energies, Urmia University of Technology, Urmia, Iran.*

[b] *Department of Chemistry, Faculty of Renewable Energies, Urmia University of Technology, Urmia, Iran*

[c] *Polymerization Engineering Department, Iran Polymer and Petrochemical Institute (IPPI), Tehran, Iran*

[d] *Laboratory for Chemical Technology (LCT), Department of Materials, Textiles and Chemical Engineering, Faculty of Engineering & Architecture, Ghent University, Belgium*

Abstract

This study utilized Semecarpus Anacardium (SA) and Quercus Infectoria (QI) nutshells as raw materials to manufacture activated carbon (AC) that is both inexpensive and possesses a large surface area. All materials were examined using Fourier transform infrared spectroscopy (FTIR), Scanning Electron Microscopy (SEM/EDX), X-ray powder diffraction (XRD), and Brunauer, Emmett, and Teller (BET) surface area methods. The effective synthesis of AC was validated by surface functional groups in FTIR spectra and XRD diffractograms, which showed a broad peak in the region of 2θ=15-28° and a faint and wide peak in the range of 2θ=40-48°. The BET results indicated that the AC synthesized from SA and activated with KOH (ACSAK) had the greatest surface area (717 m^2/g^{-1}), the most enormous pore volume (0.286 cm^3/g^{-1}), and mean pore diameters (<2nm). The synthesized AC in this research can be classified into micro-pore adsorbents entirely. Finally, the resulting ACSAK was applied to Methylene Blue (MB) adsorption. Adsorption studies demonstrate that the Langmuir isotherm (R^2=0.996) matches somewhat more accurately than the Freundlich and Temkin isotherms. Our adsorption kinetics findings show that the pseudo-second-order model has the maximum fitness and accuracy on MB adsorption data in AC (R^2 = 0.999).

Keywords: *Activated carbon, Semecarpus Anacardium, Quercus Infectoria, Methylene Blue, isotherms, kinetics.*

***Corresponding author**:

Department of Chemistry, Faculty of Renewable Energies, Urmia University of Technology, P.O.Box 57155-419, Urmia, Iran. E-mail: m.ghadiri@uut.ac.ir (M. Ghadiri), Tel.: + 98 914 400 1483, fax: + 98 44 3355 4148.

Introduction

Water pollution, removal, and recovery of pollutants from aqueous systems have received considerable attention in recent decades. Due to the adverse effects of water pollution on man-made life and the environment, there has been an increasing literature dedicated to removing water pollution [1-5]. Various pollutants cause contamination in the water and wastewater e.g. heavy metals, organic particles, inorganic particles, pharmaceutical hazardous substances, and toxins [6-10]. Methylene blue (MB) as a cationic dye is one of the dangerous water-soluble pollutants that is used in leather, tanning, and textiles which causes cancer, mutation, and skin diseases [11, 12]. Various techniques have been used to eliminate MB from a water-based system, such as adsorption, electrocoagulation flocculation, electro-dialysis, biodegradation, catalytic ozonation, and ion exchange [13-17]. Aydin et al. conducted a study on the adsorption of acid and basic dye using powdered cotton fibers [18]. Additionally, Aydin and Çifçi examined the color removal efficacy of H_3PO_4 activated cypress tree cone for the removal of MB, using both traditional and ultrasonic-assisted adsorption procedures [19]. Regarding initial costs, availability, operational capabilities, and effective separation, adsorption has been widely used to remove toxic pollutants from aquatic systems [20].

Activated carbon (AC) is well-known as the most used and efficient adsorbent due to its large surface area, fast adsorption kinetics, thermal and chemical stability, and well-developed pore structure [21]. Both the production process and the nature of precursors have a significant influence on the porous structure and adsorption properties of the resultant AC. The production process includes chemical and physical methods. Physical activation has carbonization and activation steps [22]. During carbonization, non-carbon components such as hydrogen and oxygen are removed from raw materials. Steam and/or CO_2 as oxidizing reagents are used to activate the carbonized char. Chemical activation commonly occurs at lower temperatures than physical activation based on the agent activity and chemical reagent/precursor ratio. In chemical activation, carbonaceous materials are impregnated with alkali and/or acidic reagents followed by heating the resulting slurry in an inert atmosphere. In general, chemical activation has priority over physical activation regarding lower carbonization temperature, energy saving, shorter time of activation, and narrower porosity distribution with higher controllability. Moreover, chemical activation leads to the production of ACs with higher surface area [23]. Many researchers have introduced the production of AC by chemical activation during the last few years. El Hadrami et al. used phosphoric acid as a chemical reagent to produce AC from hydrochar [24]. Said et al. studied KOH as a chemical reagent for the synthesis of AC from date seeds [25].

In the case of precursors nature, different feed-stocks have been used to produce AC (Table 1) e.g. varied agricultural wastes with low-cost and efficient adsorption. However, there is no reported study based on the production of AC from semecarpus Anacardium (SA) and Quercus Infectoria (QI) nutshells. The production of AC from SA and QI nutshells can most likely prevent leaving agricultural waste in the environment. Moreover, (SA) and (QI) nutshells have a high percentage of carbon materials.

Table 1. Previous research on the production of AC

Precursor	Activation method	Reference
Date seeds	Chemical activation	[25]
Tea residue	Chemical activation	[21]
Walnut shells	Chemical activation	[26]
Scotch pine bark	Chemical activation	[27]
Coal	Chemical activation	[28]
Jatoba fruits barks	Chemical activation	[29]
Paper sludge	Chemical activation	[30]
Cherry kernel shell	Chemical activation	[31]
tobacco waste	Chemical activation	[32]
Hydrochar	Chemical activation	[33]
Corn straw	Chemical activation	[34]
Peanut	Chemical activation	[35]
Coconut shell	Physical Activation	[36]

To describe the reduction of aqueous pollutants concentration according to the reaction time variation, adsorption kinetics is needed. Moreover, adsorption isotherms are accounted to consider the amount of adsorbate as a function of concentration at constant temperature [37]. An adsorption process starts with the external mass transfer, followed by external diffusion. First, there is an external mass transfer, and then there is an external diffusion, in an adsorption process. As the next steps, the intra-particle diffusion occurs, and eventually, the physical or chemical reaction between the adsorbate and the surface of the adsorbent. Each described phase has the potential to act as the phase that limits rate and has an impact on the process of adsorption as seen by various isotherms and kinetic models.

In this study, (SA) and (QI) nutshells were used as raw materials to produce inexpensive activated carbon (AC) with a high surface area. The carbonization process was investigated at a temperature of 600 °C under an N_2 atmosphere where H_3PO_4 and KOH were utilized as chemical reagents. The synthesized AC was employed to adsorption of MB from an aqueous solution. During the adsorption process, adsorbate trends were determined according to the adsorption kinetic models compared to the pseudo-first-order (PFO) kinetic model, pseudo-second-order (PSO) kinetic rate laws, and intra-particle diffusion model. The Langmuir, Freundlich, and Temkin models were used to obtain the adsorption isotherms. It is noted that ACSAK stands for AC produced from SA and activated by KOH, ACSAH stands for AC produced from SA and activated by H_3PO_4, ACQIK stands for AC produced from QI and activated by KOH and ACQIH stands for AC produced from QI and activated by H_3PO_4.

Materials and methods

Materials

SA and QI raw materials used for the production of AC were taken from the Kurdistan region in Iran. Potassium hydroxide (KOH, >85%, KianKaveh Pharmaceutical and Chemical Company) and ortho-phosphoric acid (H_3PO_4,85%, Fluka) were used as activating agents. Methylene blue, the compound $C_{16}H_{18}ClN_3S$ (MB, 319.85 g mol^{-1}) was supplied by Merck Company, and was used as a model organic pollutant to investigate the adsorption models. Double distilled water was used in all phases of the tests. All the chemical agents were used as received without further purification. The carbonization process was conducted in a closed steel chamber specifically designed in our laboratory to allow nitrogen to enter and exit. This chamber was placed inside a Paragon furnace model Xpress Q-11A. The setup of the closed steel chamber within the furnace ensured an inert atmosphere during carbonization, preventing unwanted reactions and preserving the integrity of the carbon structure.

Adsorbent preparation

The SA and QI nutshells were first rinsed with hot water to eliminate any soluble contaminants, and then dried in an oven at a temperature of 105 °C for the duration of the night. Precursor particles were sieved and sized less than 4mm. Chemical reagents including KOH and H_3PO_4 were used in the impregnation step. The chemical ratio (activating agent/precursor) was 100% in this case. In the impregnation step, the mixing was performed via a magnetic stirrer at 50 °C for 4 hours. The slurry was dried in an oven at a temperature of 105 °C for the whole night after being mixed.

The pyrolysis step was performed in a horizontal tube furnace with 15 cm in height and 4cm in diameter under N_2 atmosphere (150 cm^3/min). For each pyrolysis experiment, 10 g of impregnated samples was used. The heating rate, final temperature, and maintenance time were 10 °C/min, 600 °C, and 90 min, respectively. To bring the sample down to ambient temperature after carbonization, N_2 gas was used. The AC samples underwent several washes with distilled hot water, followed by oven-drying at a temperature of 105 °C for the duration of one night. The schematic diagram of the synthesis of different ACs is shown in Fig. 1.

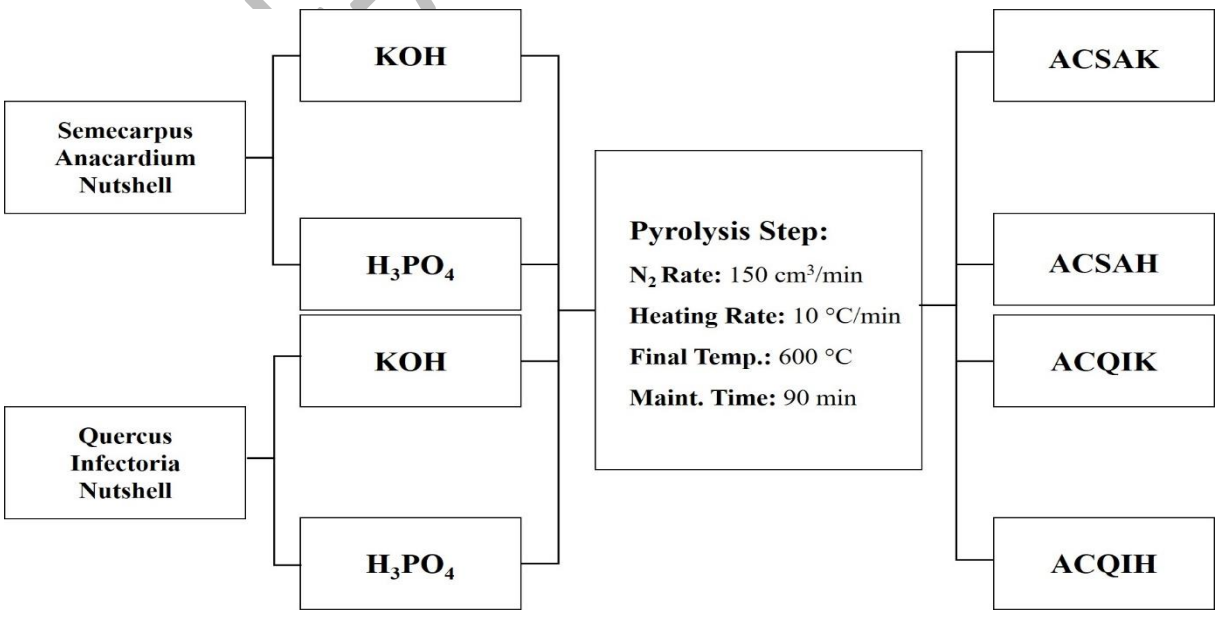

Fig. 1. Schematic diagram of AC synthesis

Batch studies

A stock solution of MB was produced at a concentration of 500 mg/L. Adsorption tests were conducted in four 250 mL Erlenmeyer flasks containing 100 mL of MB solution that was obtained from the stock solution and had a concentration of 25 mg/L. 0.2 g of each AC sample was added to solutions as follows. Following a 24-hour period, during which the mixes achieved equilibrium, the solutions were subjected to filtration, and the concentration of MB in the resulting solutions was examined. To analyze adsorption isotherms, a diverse concentration of MB was prepared, and 1 g of AC was added to solutions after equilibrium was reached. It was calculated how much MB was adsorbed for every gram of adsorbent It should be emphasized that all tests were carried out at neutral pH and ambient temperatures.

Kinetic experiments

Kinetic experiments were started with 100 ml of a solution of 55 mg/L of MB containing 1g of AC. The concentration of MB in solution per 1 g of adsorbent was evaluated after 20, 32, 44, 56, 68, 80, and 92 minutes.

Characterization

X-ray powder diffraction data from a PHILIPS/PW1730 diffractometer employing CuKα radiation (λ= 1.5418 Å) at 30 kV and 30 mA was used to determine sample crystal structure. The N_2 adsorption/desorption tests (BEL/ BELSORP MINI II) at 77 K were used to evaluate the BET porosity and surface area of all AC samples. The surface functional groups of AC samples were characterized using a Fourier transform infrared spectrometer (FTIR, Thermo/AVATAR) by KBr pellets containing 1.0 wt. % of the samples. To investigate the AC morphology, scanning electron microscopy (SEM) images with TESCAN - MIRA III equipped with an EDX energy dispersive analysis (EDX) system are performed on gold-coated samples to reduce costs. Ultraviolet-visible spectrophotometer (UV-Vis) data collected by an Optima INC-SP300DB UV–Vis spectrophotometer were performed on synthesized AC. The UV wavelength was set at 665 nm to quantify the amount of MB adsorbed on AC samples.

Results and discussion

Effect of raw materials and chemical reagents

Four samples of AC were synthesized by two kinds of raw materials and chemical reagents. All samples were exerted to adsorb MB from an aqueous solution, and the outcomes are recorded in Table 2 According to the data shown in Table 2, SA is a more appropriate raw material than QI for the synthesis of AC. Chemical reagents have an operative effect on synthesized AC; however, the performance of chemical reagents depends on the raw material. According to the adsorption experiments, KOH and H_3PO_4 are well-suited for SA and QI, respectively.

Table 2. Quantitative results of MB adsorption on AC

Raw materials	Abb.	Chemical reagents	Dye	The initial concentration of dye (ppm)	Amount of dye adsorbed (ppm)
SA	ACSAK	KOH	MB	25	19.4
SA	ACSAH	H_3PO_4	MB	25	16.5
QI	ACQIK	KOH	MB	25	8.1
QI	ACQIH	H_3PO_4	MB	25	10

XRD analysis

An X-ray diffraction graph of the SA and AC has the highest surface area (ACSAK) is seen in Fig. 2. The relatively distinct diffraction peak of the SA shell sample at about 2θ =16° and 34° compared to that of obtained AC indicates that carbonization can produce AC with a highly amorphous nature. The produced AC sample (ACSAK) displayed XRD patterns with a large peak in the 15–28° range of 2θ scale and a weak and broad peak in the 40–48° range of 2θ scale, originating from the (002) and (100) planes, respectively. The intensity of these peaks is indicative of the degree of graphitization of the AC, with higher intensity peaks corresponding to higher degrees of graphitization. This is significant because the degree of graphitization of AC affects its properties, such as its surface area, porosity, and electrical conductivity. It may be attributed to the randomly formed amorphous arrangements of carbon with disordered built up carbon rings and the low concentration of crystalline graphite, respectively [38, 39]. The presence of microspores in the samples scattered the X-ray beam between 15 and 28° and caused a decrease in the crystallinity and an increase in the amorphous background [40]. The XRD data shown in Fig. 2 indicate that both ACSAK and MB-ACSAK samples possess the XRD peaks characteristic of AC. As seen in XRD patterns, there is no noticeable difference between these samples, suggesting that the MB adsorption on AC does not affect the microstructure of prepared carbon materials. As seen in Fig. 2, the intensities of the reflections are only slightly changed, indicating that the main features of the AC structure are preserved.

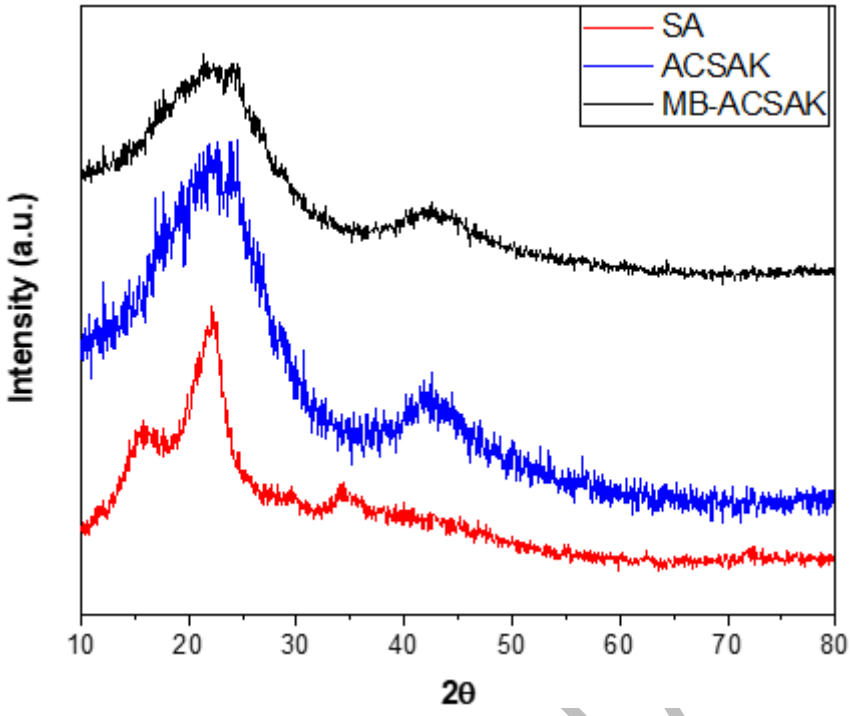

Fig. 2. XRD patterns of SA, ACSAK, and MB-ACSAK powder samples

FT-IR analysis

The FTIR method was used to evaluate the surface functional groups of both the source materials and the produced ACs. The FTIR spectra of QI and SA precursors, ACQIH, and ACSAK prepared AC and MB adsorbed ACSAK samples are shown in Fig. 3. For ease of comparison, the FTIR spectrum of SA and QI nutshells are also included. As shown, most of the samples exhibit similar IR peaks.

The AC samples represented four important absorption peaks at 2900-3500 cm^{-1}, 1300-1730 cm^{-1}, 1000-1250 cm^{-1} and 450-700 cm^{-1}. A broad stretching band at around 3400 cm^{-1} is mainly caused by the hydroxyl groups' vibration of the adsorbed water molecules on the surface of nutshells and ACs after carbonization. Absorption peaks appearing at 2850 to 2925 cm^{-1} for all samples suggest the presence of CH stretching vibration and CH_2 asymmetrical vibrations.

For ACSAK, the band at about 1626 cm^{-1} is attributed to the tensile vibration of C = O, which has decreased in comparison to the raw crust probably due to KOH water scarcity [41]. The weak band at 1524 cm^{-1} for QI and SA samples, in short, indicates the presence of C = C bonds of aromatic compounds after carbonization cannot be observed for ACQIH and ACSAK-activated samples [42].

The FTIR spectrum of synthetic carbons ACQIH and ACSAK at around 1454 cm^{-1} shows absorption bands due to –CH– deformation. The peak at around 1383 cm^{-1} is assigned to the bending vibrations of the methyl group [43]. The broadband observed in the region of 1000 to 1250 cm^{-1} is related to a characteristic absorption of the hydroxyl (–OH) group. These results are consistent with the findings of many researchers [44]. The vibrations of in-plane and out-of-plane aromatic ring deformations have a peak in about the 480-485 cm^{-1} range [45]. The presence and intensity of these peaks can provide insights into the surface chemistry of the AC. For example, the intensity of the O-H stretching peak is indicative of the number of hydroxyl groups on the surface of the AC, which can affect its hydrophilicity and adsorption properties. The presence of the C=O and C-O stretching peaks

is indicative of the presence of oxygen-containing functional groups, which can also affect the adsorption properties of the AC.

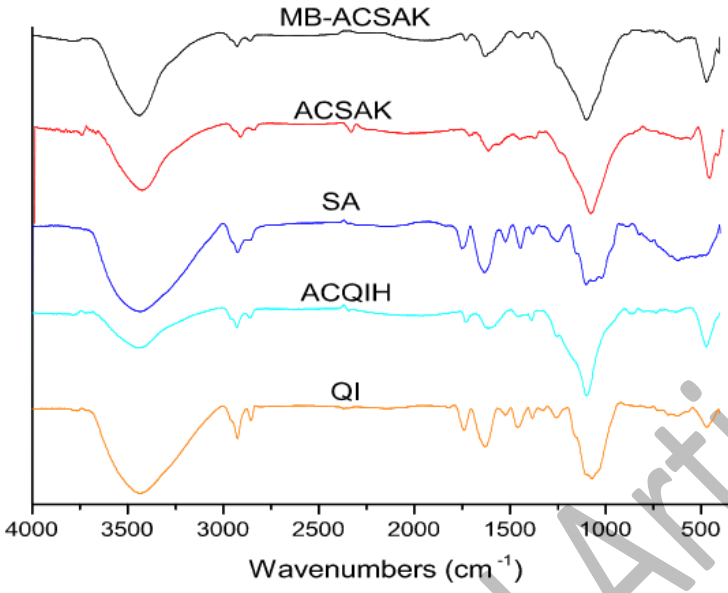

Fig. 3. FTIR spectra of parent materials (QI, SA), corresponding ACs (ACQIH, ACSAK) and MB adsorbed ACSAK (MB-ACSAK)

Analysis of adsorption-desorption isotherms

The results of the N_2 adsorption-desorption experiments are displayed in Fig. 4, which exhibits type I isotherm according to Brunauer's classification for synthesized samples entirely. Type I represents micropores, including pores with a diameter below 2 nm. Two samples derived from QI have a hysteresis loop in their adsorption-desorption plots, which implies that these samples have mesoporous structures. The type of this loop can be related to the shape of the pores. Thus, a classical open cylindrical or tabular pore shape was expected according to the form of the hysteresis loop.

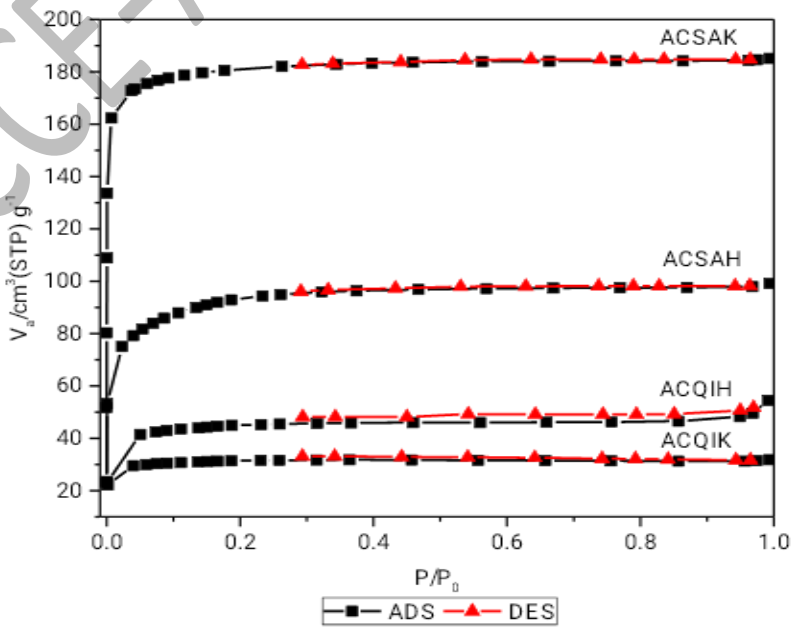

Fig. 4. ADS-DES plot of ACSAK, ACSAH, ACQIK, and ACQIH samples

BET results

The BET analyses determine the physical characteristics and porosity of the adsorbents. N_2 adsorption-desorption isotherms provide measurements for specific surface area, pore diameter, and total pore volume. Fig. 4 illustrates the adsorption-desorption isotherms and Table 3 lists the surface properties of the AC derived from SA and QI. Table 3 shows BET results including, total pore volume, BET surface area, and mean pore diameters of the prepared AC. The results indicated that AC synthesized from SA has a higher surface area than AC synthesized from QI nutshells.

Table 3. N_2 sorption and chemical analysis of AC produced from Semecarpus Anacardium and Quercus Infectoria

Sample	S_{BET} ($m^2.g^{-1}$)	Total pore volume ($cm^3\ g^{-1}$)	Mean pore diameter (nm)	Elemental analysis (wt.%)					
				C	N	O	S	K	P
SA	-	-	-	44	11.3	44.1	0.08	0.52	0.06
ACSAK	717.59	0.2863	1.5956	72.2	14.5	12.5	0.17	0.62	-
ACSAH	337.89	0.1531	1.8126	-	-	-	-	-	-
ACQIK	122	0.04919	1.6127	-	-	-	-	-	-
ACQIH	170.46	0.08365	1.963	-	-	-	-	-	-

KOH as the chemical reagent was significantly more efficient than H_3PO_4 for activating the AC prepared from SA. Consequently, the ACSAK had the best characters among all the samples. KOH plays an important role in the pore-making process of activated carbon, resulting in a high surface area. When KOH is mixed with the carbon precursor and heated, a series of chemical reactions occur. These reactions break down the carbon structure and create new pores. The KOH also reacts with the carbon to form potassium carbonate (K_2CO_3), which acts as a catalyst and further enhances the pore-making process.

KOH also removes water and hydrogen from the carbon precursor, which leads to the formation of pores and reacts with the carbon precursor to form carbon monoxide and hydrogen gas. These gases are then released from the carbon, creating new pores [46].

Barrett-Joyner-Halenda (BJH) analysis results showed that mean pore diameters were below 2 nm for all samples; in other words, synthesized AC in this research could be classified into micropore adsorbents entirely. Fig. 5 includes BJH figures and presents the pore size distribution in samples of produced AC. This figure reveals that ACQIK and ACQIH were mesopores materials that can be referred to the raw materials.

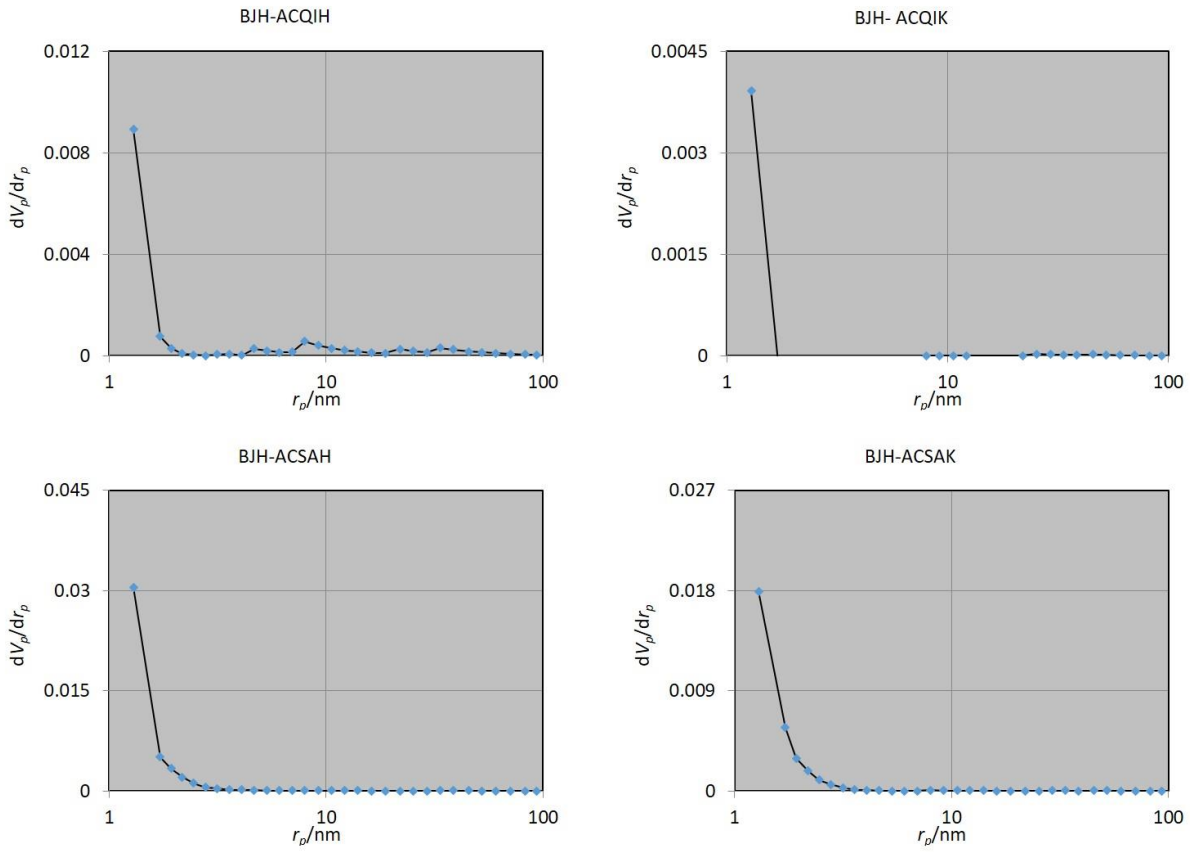

Fig. 5. BJH plots of AC produced from SA and QI

Microscopic structure and chemical analysis of the AC

EDX analysis was used to investigate the chemical constituents of the SA and ACSAK samples. Table 3 displays the outcomes of the comprehensive analysis. The SA nutshell used mainly contains carbon (44%), nitrogen (11.3%), and oxygen (44.1%), as expected like most lignocellulose materials. The elemental composition ACSAK sample is given in Table 3. The data shown in Table 3 clearly demonstrates that the use of KOH as an activating agent had a substantial impact on the production of ACs with a high carbon content (72.2%). After the activation process, the carbon contents of the activated sample significantly increased compared to the SA nutshell raw material, and the Oxygen contents, unlike Carbon, will decrease after activation as expected.

In the activation and pyrolysis processes, SA nutshell decomposed and as a result, volatile compounds that contain mostly oxygen and phosphorus were released resulting in a carbon-rich product. The SEM was used to study the surface appearance and basic physical parameters of AC that were synthesized from SA and its matching MB-loaded AC. Fig. 6 presents the SEM images of both ACSAK and ACSAK-MB. As can be seen from Fig. 6 there is a difference between ACSAK and ACSAK-MB materials. The surface of ACSAK demonstrates a well-developed porous media, including great pores with high surface area and cracks.

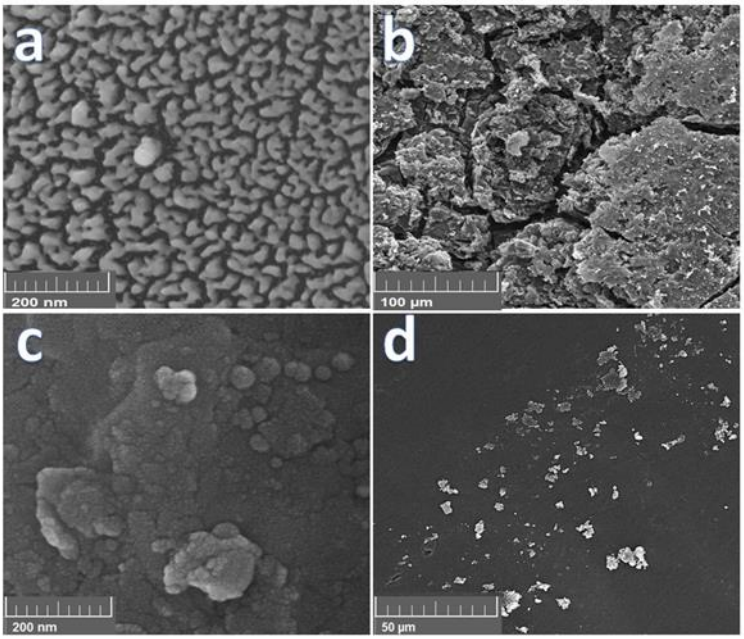

Fig. 6. Microscopic structure analysis of the activated carbon ACSAK(a-b) and MB-ACSAK(c-d).

This unique microporous structure observed contains pores with varied sizes and shapes that have a channel role for the network of adsorbents. Whereas the SEM images of ACSAK-MB represent that the surface of the adsorbent has been covered by adsorbate and dye molecules have formed a film masking the pores and aggregates which the pore structure of the adsorbent cannot be seen.

Adsorption isotherms

The adsorption isotherms were evaluated by employing the Langmuir, Freundlich, and Temkin isotherm models. The values of isotherm model parameters were calculated from each model's linear graph. The linear graphs were traced according to the linear mathematical expressions of isotherm models, respectively. The Langmuir model supposes that monolayer adsorption occurs at the adsorbent's sites with no lateral interactions between the molecules adsorbed, the surface is homogeneous energetically and all adsorption sites are active equally. The linear equation of the Langmuir isotherm model is [47,48]:

$$\left(\frac{C_e}{q_e}\right) = \left(\frac{1}{k_L q_m}\right) + \left(\frac{C_e}{q_m}\right) \qquad (1)$$

where the C_e (mg. L^{-1}) is the dye concentration in equilibrium, q_e (mg. g^{-1}) is the amount of adsorbate that can be absorbed per unit mass of adsorbent, q_m (mg. g^{-1}) is the maximum adsorption capacity and k_L (L. mg^{-1}) is the Langmuir constant, which refers to the adsorbent/adsorbent affinity. The regression of the plot $\left(\frac{C_e}{q_e}\right)$ versus C_e provides a slope $\left(\frac{1}{q_m}\right)$ and intercept of $\left(\frac{1}{k_L q_m}\right)$ of the straight line, respectively.

For the heterogeneous surface, the Freundlich isothermal model is used that defines multilayer adsorption not only for mono-layer distribution. It expresses the relationship between the solute concentration on the adsorbent and the solute concentration in the liquid. The linearized equation of the Freundlich model [49] is:

$$logq_e = log\, k_f + \left(\frac{1}{n}\right) logC_e \quad (2)$$

where k_f denotes the adsorbent's sorption capacity constant. Moreover, it points out the affinity between the species. 'n' denotes the Freundlich constants that take into account the adsorption rate influencing factor. The slope of the linear plot of $logq_e$ against log C_e gives the (1/n), where the intercept of the same plot provides $logk_f$. According to the Temkin isotherm model, as the surface area of the adsorbent increases, the adsorption of all molecules decreases linearly, and adsorption is measured by the uniform distribution of binding energies up to the maximal binding energy. The linear form of the Temkin model is written as [49]:

$$Q_e = \left(\frac{RT}{bT}\right) lnk_T + \left(\frac{RT}{bT}\right) lnC_e \quad (3)$$

B= (RT/b_T) is considered as the heat adsorption in ($J.mol^{-1}$), where R is the gas constant (8.3145 $J.mol^{-1}$. K^{-1}), T (K) is the absolute temperature, b_T ($J.mol^{-1}$) is Temkin constant adsorption thermal-based and k_T ($L.g^{-1}$) is the Temkin isotherm equilibrium binding constant. The plot of Q_e against lnC_e reveals B and A_T as the slope and intercept of the figure, respectively.

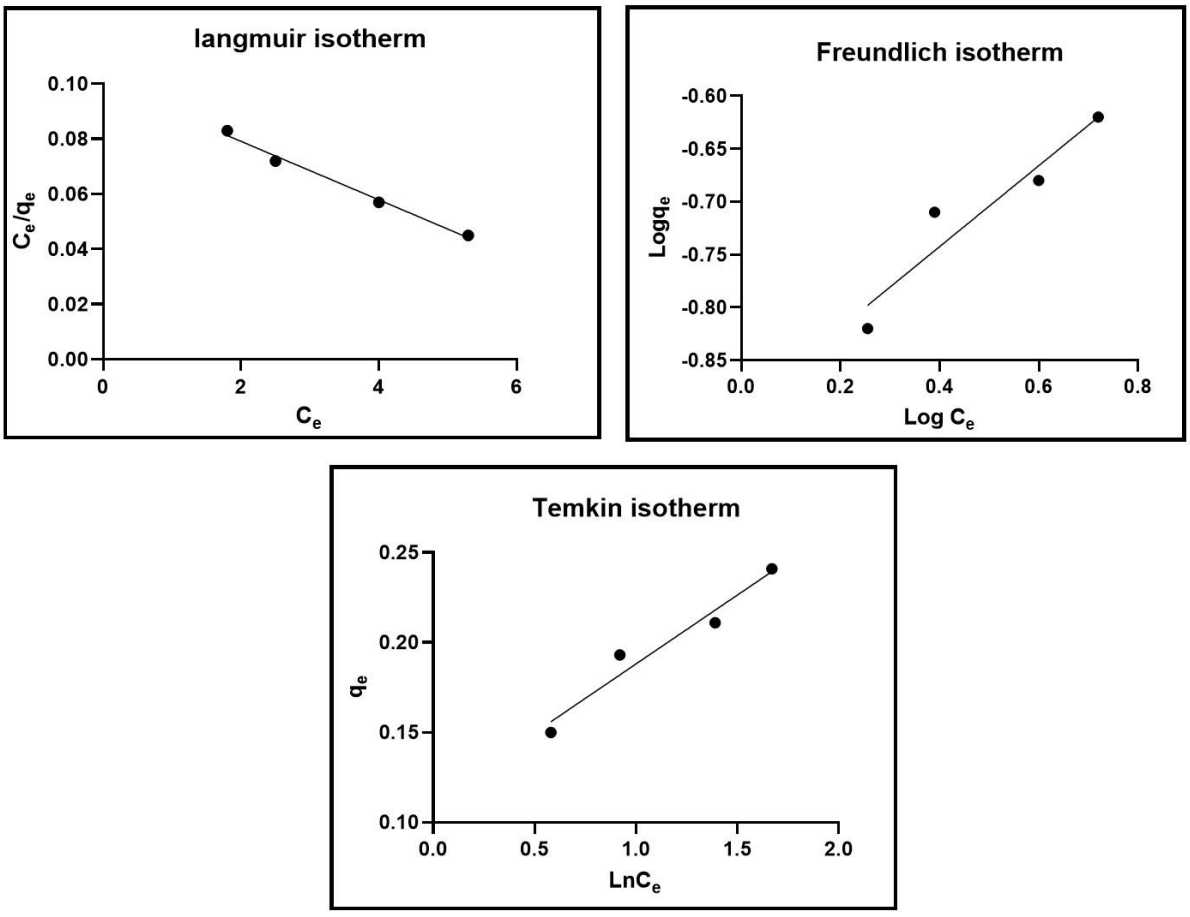

Fig. 7. Plots o Langmuir, Freundlich, and, Temkin model of MB adsorption on the AC

The adsorption of MB on the ACSAK was exerted in four different concentrations 32, 39, 46, and 53 (mg. L^{-1}) to evaluate the adsorption isotherms. The residual concentration of MB was measured utilizing a UV-vis spectrophotometer at 665 nm. Quantitative results of adsorption isotherms have been listed in Table 4, which have been calculated from Fig. 7.

According to Table 4, k_L and q_m have been calculated as 2.06 $L.mg^{-1}$ and 3.258 $mg.g^{-1}$ respectively. Table 6 summarizes a comparative evaluation of the MB adsorption capacities of different Acs.

However, the calculation of the related correlation coefficient points out that all three models yielded a good fit on experimental data. The Langmuir isotherm had a somewhat better fit than the Freundlich and Temkin isotherms. k_f and n derived from the Freundlich equation were 1.24 and 2.591, respectively. The value of n was more significant than unity, which indicated the optimal absorption of MB in AC. The high value of the correlation coefficient showed good linearity of the Temkin isotherm model, where the k_T was determined with a value of 4.3 $L.g^{-1}$ and B was equal to 0.75 $J.mol^{-1}$.

75 $J.mol^{-1}$.

Table 4. Adsorption parameters of adsorption equilibrium models

Langmuir model			Freundlich model			Temkin model		
q_m ($mg.g^{-1}$)	k_L ($L.mg^{-1}$)	R^2	n	k_f $(mg/g)(L/mg)^{1/n}$	R^2	B ($j.mol^{-1}$)	k_T ($L.g^{-1}$)	R^2
3.258	2.06	0.996	2.591	1.24	0.993	0.75	43	0.994

Table 5. Comparison of MB maximum adsorption capacity on to activated carbon prepared from various precursors.

Precursor	q_m ($mg.g^{-1}$)	Reference
Semecarpus anacardium	3.258	This study
Guinea corn stem carbon	0.259	[50]
Maize cob carbon	0.325	[50]
Coconut shell	0.455	[50]
Corncob-activated carbon	0.84	[51]
Almond shell	1.33	[52]
Walnut shell	3.53	[52]

Kinetic studies

To explain the rate and process of the adsorption, the PFO equation, PSO equation, and intra-particle model were investigated. The PFO assumes that the rate of adsorption is based on adsorption capacity as:

$$\frac{dq_t}{dt} = K_1(q_e - q_t) \quad (4)$$

The linearized equation is as:

$$ln\,(q_e - q_t) = ln\,q_e - \frac{tK_1}{2.303} \quad (5)$$

Where q_e (mg/g) and q_t (mg/g) are the quantities of adsorbate adsorbed at equilibrium and any time, respectively, t (h) is time, and K_1 (1/h) is the adsorption rate constant. A straight line with slope and intercept of $K_1/2.303$ and lnq_e is obtained by regressing the plot ln (q_e- q_t) against 't'. The PSO describes that the rate of the adsorption is proportional to the square of the difference between amounts of adsorbate variable with time and amounts of adsorbate at equilibrium as [53]:

$$\frac{dq_t}{dt} = K_1(q_e - q_t)^2 \quad (6)$$

The linearized form of the equation is as:

$$\frac{t}{q_t} = \frac{1}{K_2 q_e^2} + \frac{t}{q_e} \quad (7)$$

Where K_2 (g/mg. h) is the rate constant of the second-order adsorption. To be noted the assumptions are almost the same in both kinetic models except that in the PSO model, the adsorption of the adsorbate on the adsorbent is regulated by the second-order rate equation. The t/q_t and t linear plot slope and interception are as $1/q_e$ and $1/K_2qe^2$, respectively, which helps to find the K_2 and q_e. Whereas the intra-particle model assumes that internal diffusion controls the adsorption process. The intra-particle diffusion includes three steps, including:

1- Diffusion of the adsorbate through the bulk of the solution
2- Diffusion through the film around the adsorbent
3- Diffusion through the micropores and macrospores of the adsorbent

Each step can be the limiting step. By the way, the intra-particle diffusion equation can be written as [53]:

$$q_t = K_i\, t^{0.5} + C \quad (8)$$

Where K_d (mg/g.$h^{0.5}$) is the intra-particle diffusion equation constant, which can be obtained from the slope of the linear plot of q_t against $t^{0.5}$. C is the intercept of the current plot which indicates the depth of the boundary layer. The adsorption kinetics of MB with ACSAK was investigated in 20, 32, 44, 56, 68, 80, and 92 minutes. Quantitative results of adsorption kinetics have been listed in Table 6 which is calculated from linearized figures of each kinetic model in Fig. 8.

By investigation of quantitative results of adsorption kinetics can be obtained that the PSO model had the best fitness and accuracy on adsorption data of MB on AC, and the rate of the adsorption was proportional to the square of the difference between several adsorbate variables with time and number of adsorbates at equilibrium. Due to the gap and duality of the intra-particle diffusion model, it can be concluded that the absorption process consists of almost two or more steps. The first step shows the adsorption of dye on the adsorbent, which occurs immediately. The second stage describes the penetration of dye into adsorption sites gradually, where the intra-particle diffusion controls the adsorption process.

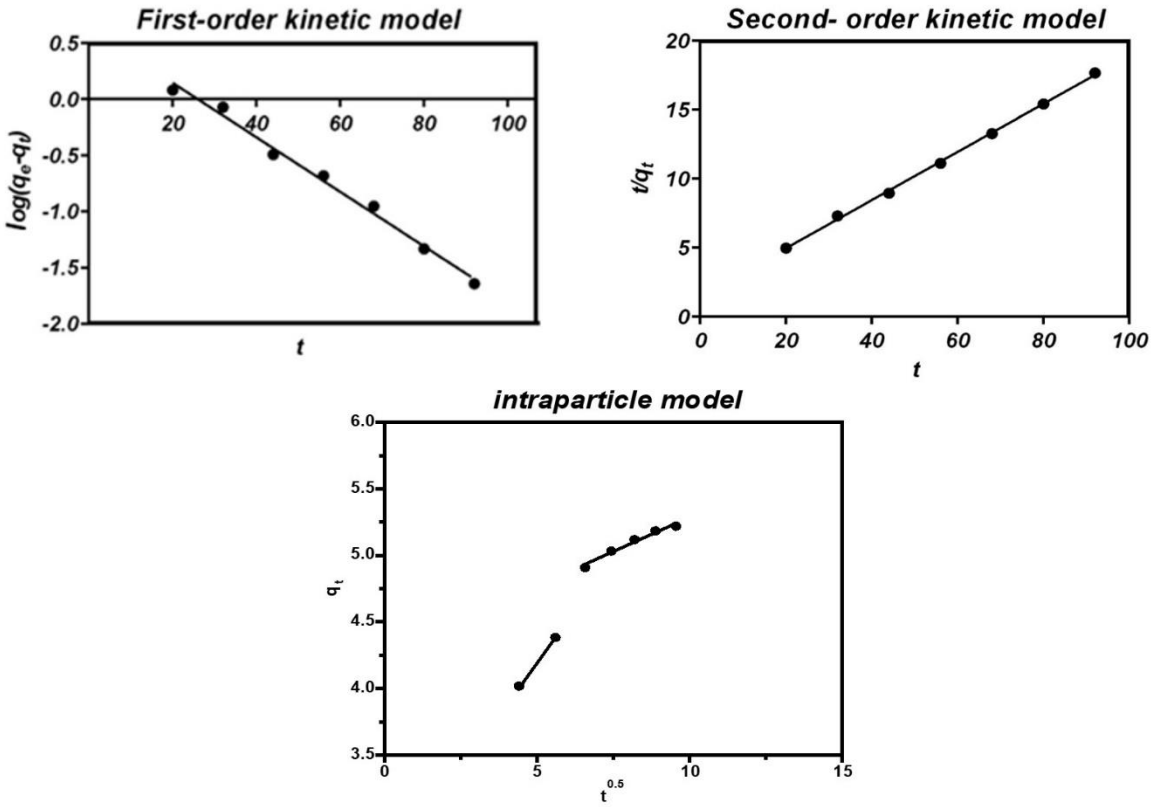

Fig. 8. Plots of PFO, PSO, and, intra-particle models of MB adsorption on the AC

Table 6. Quantitative results of adsorption kinetics of MB on AC

Pseudo-first-order			Pseudo-second-order			Intraparticle		
q_c(mg/g)	K_1 (1/h)	R^2	q_c(mg/g)	K_2(g/mg.h)	R^2	C	K_i(mg/g.$h^{0.5}$)	R^2
4.295	0.055	0.991	5.71	40.22	0.999	4.248	0.103	0.96

Conclusion

The AC was successfully synthesized from SA and QI nutshells as practical and low-cost materials. The synthesized ACs were characterized using XRD, FTIR, SEM/EDX, and BET surface area techniques. The results showed that SA nutshells had higher adsorption capacity than QI nutshells. In other words, SA nutshells activated by KOH (ACSAK) were a well-suited and cost-effective adsorbent with a higher surface area (717 $m^2.g^{-1}$), highest pore volume (0.2863 $cm^3.g^{-1}$) and lowest mean pore diameter (1.5956 nm). Isotherm data were significantly correlated with the Langmuir isotherm model (R^2=0.996). Kinetic studies showed that PSO had the highest fitting on the adsorption experiments (R^2= 0.999). This research exhibits that SA can be a suitable source for AC preparation, and the resulting adsorbent can be a cost-effective adsorbent with a high surface area which is appropriate for adsorption of water and wastewater pollutions.

References

1. Azimi, S. C., Shirini, F., & Pendashteh, A. R., Advanced oxidation process as a green technology for dyes removal from wastewater: A review. Iran. J. Chem. Chem. Eng. (IJCCE), **40**(5): 1467-1489 (2021).
2. He, M., Xu, Z., Hou, D., Gao, B., Cao, X., Ok, Y. S., ... & Tsang, D. C., Waste-derived biochar for water pollution control and sustainable development. Nat. Rev. Earth Environ., **3**(7): 444-460 (2022).
3. Tarus, B. K., Jande, Y. A., & Njau, K. N., Electrospun carbon nanofibers for use in the capacitive desalination of water. New Carbon Mater., **37**(6)" 1066-1084 (2022).
4. Naghizadeh, A., & Ghafouri, M., Synthesis of low-cost Nanochitosan from Persian gulf shrimp Shell for efficient removal of reactive blue 29 (RB29) dye from aqueous solution. Iran. J. Chem. Chem. Eng. (IJCCE), **38**(6): 93-103 (2019).
5. Ghadiri, M., Hallajzadeh, J., Akhghari, Z., Nikkhah, E., Othman, H. O., Green Synthesis and Antibacterial Effects of Silver Nanoparticles on Novel Activated Carbon, Iran. J. Chem. Chem. Eng.(IJCCE), 2023; (): -. doi: 10.30492/ijcce.2023.1972151.5712
6. Bennabi, S., & Mahammed, N., Kinetic and Thermodynamic Study of Methyl Orange Dye Adsorption on Zinc Carbonyldiphthalate, an Organometallic-Based Material Prepared with a Montmorillonite Clay. Iran. J. Chem. Chem. Eng. (IJCCE), **42**(1): 123-138 (2023).
7. Modarresi-Motlagh, S., Bahadori, F., Ghadiri, M., Afghan, A., Enhancing Fenton-like oxidation of crystal violet over Fe/ZSM-5 in a plug flow reactor, Reac Kinet Mech Cat, **133**: 1061–1073 (2021).
8. Gan, Y., Ding, C., Xu, B., Liu, Z., Zhang, S., Cui, Y., ... & Song, X., Antimony (Sb) pollution control by coagulation and membrane filtration in water/wastewater treatment: A comprehensive review. J. Hazard. Mater., **442**: 130072 (2023).
9. Mehra, S., Saroha, J., Rani, E., Sharma, V., Goswami, L., Gupta, G., ... & Sharma, S. N., Development of visible light-driven SrTiO3 photocatalysts for the degradation of organic pollutants for waste-water treatment: Contrasting behavior of MB & MO dyes. Opt. Mater., **136**: 113344 (2023).
10. Barasarathi, J., Abdullah, P. S., & Uche, E. C., Application of magnetic carbon nanocomposite from agro-waste for the removal of pollutants from water and wastewater. Chemosphere, **305**: 135384 (2022).
11. Oladoye, P. O., Ajiboye, T. O., Omotola, E. O., & Oyewola, O. J., Methylene blue dye: Toxicity and potential technologies for elimination from (waste) water. Result. Engi, **16**: 100678 (2022).
12. Vedula, S. S., & Yadav, G. D., Wastewater treatment containing methylene blue dye as pollutant using adsorption by chitosan lignin membrane: Development of membrane, characterization and kinetics of adsorption. J. Indian Chem. Soc., **99**(1): 100263 (2022).

13. Marrakchi, F., Ahmed, M. J., Khanday, W. A., Asif, M., & Hameed, B. H., Mesoporous-activated carbon prepared from chitosan flakes via single-step sodium hydroxide activation for the adsorption of methylene blue. Int. J. Biol. Macromol., **98**: 233-239 (2017).
14. Mandanipour, V., Sadeghi-Maleki, M. R., & Pasandideh-Nadamani, M., Preparation of adsorbents containing CdS quantum dots from the orange peel for the sewage treatment. Iran. J. Chem. Chem. Eng., **40**(3): 704-714 (2021).
15. Ghasemzadeh, N., Ghadiri, M., Behroozsarand, A., Optimization of chemical regeneration procedures of spent activated carbon, Advances in Environmental Technology (AET), **3**(1): 45-51 (2017).
16. Salem, S., Nouri, B., Ghadiri, M., Photoactivity of magnesium aluminate under solar irradiation for treatment of wastewater contaminated by methylene blue: Effect of self-combustion factors on spinel characteristics, Sol. Energ. Mat. Sol. C, **218**: 110773 (2020).
17. Foroutan, R., Peighambardoust, S. J., Ghojavand, S., Foroughi, M., Ahmadi, A., Bahador, F., & Ramavandi, B., Development of a magnetic orange seed/Fe_3O_4 composite for the removal of methylene blue and crystal violet from aqueous media. Biomass Conv. Bioref. (2023). https://doi.org/10.1007/s13399-023-04692-x
18. Çifçi, D.İ., AYDIN, N., Atav, R., Güneş, Y., Güneş, E., Synthesis of $ZnCl_2$ Activated Raising Powder of Cotton Fabrics for Acid and Basic Dye Adsorption: A Way to Reuse Cellulosic Wastes for Sustainable Production, J. Nat. Fibers, **19**:16 14299-14317 (2022).
19. Aydın, N., Çifçi, D.İ., Comparison of Conventional and Ultrasonic-Assisted Adsorption Processes by Using H_3PO_4 Activated Cypress Tree Cone for Methylene Blue Removal, J. Water Chem. Technol. **44**: 269–279 (2022).
20. Fan, X., Peng, L., Wang, X., Han, S., Yang, L., Wang, H., & Hao, C., Efficient capture of lead ion and methylene blue by functionalized biomass carbon-based adsorbent for wastewater treatment. Ind Crops Prod, **183**: 114966 (2022).
21. Bai, X., Quan, B., Kang, C., Zhang, X., Zheng, Y., Song, J., ... & Wang, M., Activated carbon from tea residue as efficient absorbents for environmental pollutant removal from wastewater. Biomass Convers. Biorefin, **13**(15): 13433-13442 (2023).
22. Krishnamoorthy, R., Govindan, B., Banat, F., Sagadevan, V., Purushothaman, M., & Show, P. L., Date pits activated carbon for divalent lead ions removal. J. Biosci. Bioeng, **128**(1): 88-97 (2019).
23. Sujiono, E. H., Zabrian, D., Zharvan, V., & Humairah, N. A., Fabrication and characterization of coconut shell activated carbon using variation chemical activation for wastewater treatment application. Results Chem, **4**: 100291 (2022).

24. El Hadrami, A., Ojala, S., & Brahmi, R., Production of activated carbon with tunable porosity and surface chemistry via chemical activation of hydrochar with phosphoric acid under oxidizing atmosphere. Surf. Interfaces, **30**: 101849 (2022).
25. Said, B., Bacha, O., Rahmani, Y., Harfouche, N., Kheniche, H., Zerrouki, D., ... & Henni, A., Activated carbon prepared by hydrothermal pretreatment-assisted chemical activation of date seeds for supercapacitor application. Inorg. Chem. Commun, **155**: 111012 (2023).
26. Ghoualem, H., & Bougheriou, F., Synthesis and characterization of activated carbons from walnut shells to remove Diclofenac. Iran. J. Chem. Chem. Eng. (IJCCE), 2023; (): -. doi: 10.30492/ijcce.2023.559588.5499.
27. Aral, S. Production of effective activated carbon from scotch pine bark and investigation of the adsorption properties. Iran. J. Chem. Chem. Eng. (IJCCE), 2023; (): -. doi: 10.30492/ijcce.2023.1995732.5912.
28. Wazir, A. H., Haq, I. U., Manan, A., & Khan, A., Preparation and characterization of activated carbon from coal by chemical activation with KOH. Int. J. Coal Prep. Util., **42**(5): 1477-1488 (2022).
29. Spessato, L., Bedin, K. C., Cazetta, A. L., Souza, I. P., Duarte, V. A., Crespo, L. H., ... & Almeida, V. C., KOH-super activated carbon from biomass waste: Insights into the paracetamol adsorption mechanism and thermal regeneration cycles. J. hazard. Mater., **371**: 499-505 (2019).
30. Jaria, G., Silva, C. P., Oliveira, J. A., Santos, S. M., Gil, M. V., Otero, M., ... & Esteves, V. I., Production of highly efficient activated carbons from industrial wastes for the removal of pharmaceuticals from water—A full factorial design. J. Hazard. Mater., **370**: 212-218 (2019).
31. Khuder, A., Koudsi, Y., Abboudi, M., & Aljoumaa, K., Removal of Cr (III), Mn (II), Fe (III), Ni (II), Cu (II), Zn (II), and Pb (II) from water solutions using activated carbon based on cherry kernel shell powder, Iran. J. Chem. Chem. Eng. Research Article Vol, **41**(11): 3687-3705 (2022).
32. Chen, H., Guo, Y. C., Wang, F., Wang, G., Qi, P. R., Guo, X. H., ... & Yu, F., An activated carbon derived from tobacco waste for use as a supercapacitor electrode material. New Carbon Mater., **32**(6): 592-599 (2017).
33. Sevilla, M., Ferrero, G. A., & Fuertes, A. B., Beyond KOH activation for the synthesis of superactivated carbons from hydrochar. Carbon, **114**: 50-58 (2017).
34. Ma, H., Yang, J., Gao, X., Liu, Z., Liu, X., & Xu, Z., Removal of chromium (VI) from water by porous carbon derived from corn straw: Influencing factors, regeneration and mechanism. J. Hazard. Mater, **369**: 550-560 (2019).
35. Zafar, M. N., Ghafoor, S., Tabassum, M., Zubair, M., Nazar, M. F., & Ashfaq, M., Utilization of peanut (Arachis hypogaea) hull based activated carbon for the removal of amaranth dye from aqueous solutions. Iran. J. Chem. Chem. Eng. (IJCCE), **39**(4): 183-191 (2020).

36. Sun, K., Leng, C. Y., Jiang, J. C., Bu, Q., Lin, G. F., Lu, X. C., & Zhu, G. Z., Microporous activated carbons from coconut shells produced by self-activation using the pyrolysis gases produced from them, that have an excellent electric double layer performance. New Carbon Mater, **32**(5): 451-459 (2017).

37. Konggidinata, M. I., Chao, B., Lian, Q., Subramaniam, R., Zappi, M., & Gang, D. D., Equilibrium, kinetic and thermodynamic studies for adsorption of BTEX onto Ordered Mesoporous Carbon (OMC). J. Hazard. Mater, **336**: 249-259 (2017).

38. Tang, Y. B., Liu, Q., & Chen, F. Y. Preparation and characterization of activated carbon from waste ramulus mori. Chem. Eng. J, **203**: 19-24 (2012).

39. Zhao, J., Yang, L., Li, F., Yu, R., & Jin, C., Structural evolution in the graphitization process of activated carbon by high-pressure sintering. Carbon, **47**(3): 744-751 (2009).

40. Mangun, C. L., Benak, K. R., Economy, J., & Foster, K. L., Surface chemistry, pore sizes and adsorption properties of activated carbon fibers and precursors treated with ammonia. Carbon, **39**(12): 1809-1820 (2001).

41. Zhong, Z. Y., Yang, Q., Li, X. M., Luo, K., Liu, Y., & Zeng, G. M., Preparation of peanut hull-based activated carbon by microwave-induced phosphoric acid activation and its application in Remazol Brilliant Blue R adsorption. Ind Crops Prod, **37**(1): 178-185 (2012).

42. Hsu, C. F., Zhang, L., Peng, H., Travas-Sejdic, J., & Kilmartin, P. A., Free radical scavenging properties of polypyrrole and poly (3, 4-ethylenedioxythiophene). Curr Appl Phys, **8**(3-4): 316-319 (2008).

43. Inam, E. I., Etim, U. J., Akpabio, E. G., & Umoren, S. A., Simultaneous adsorption of lead (II) and 3, 7-Bis (dimethylamino)-phenothiazin-5-ium chloride from aqueous solution by activated carbon prepared from plantain peels. Desalin. Water Treat, **57**(14): 6540-6553 (2016).

44. Attia, A. A., Rashwan, W. E., & Khedr, S. A., Capacity of activated carbon in the removal of acid dyes subsequent to its thermal treatment. Dyes Pigm, **69**(3): 128-136 (2006).

45. M.R., Infrared characteristic group frequencies: G. Socrates, John Wiley & Sons, Chichester, New York, Brisbane, Toronto, (1980).

46. Williams, N.E., Oba, O.A. and Aydinlik, N.P., Modification, Production, and Methods of KOH-Activated Carbon, CBEN, **9**: 164-189 (2022).

47. Ghosal, P. S., & Gupta, A. K., Determination of thermodynamic parameters from Langmuir isotherm constant-revisited, J. Mol. Liq, **225**: 137-146 (2017).

48. Darweesh, M. A., Elgendy, M. Y., Ayad, M. I., Ahmed, A. M., Elsayed, N. K., & Hammad, W. A., Adsorption isotherm, kinetic, and optimization studies for copper (II) removal from aqueous solutions by banana leaves and derived activated carbon. S. Afr. J. Chem. Eng, **40**:10-20 (2022).

49. Dada, A. O., Olalekan, A. P., Olatunya, A. M., & Dada, O. J. I. J. C., Langmuir, Freundlich, Temkin and Dubinin–Radushkevich isotherms studies of equilibrium sorption of Zn^{2+} unto phosphoric acid modified rice husk. IOSR J. Appl. Chem, **3**(1): 38-45 (2012).

50. Fo, O., & Odebunmi, E. O., Freundlich and Langmuir isotherms parameters for adsorption of methylene blue by activated carbon derived from agrowastes. Adv. nat. appl. sci., **4**, 281-288 (2010).

51. Tseng, R. L., Tseng, S. K., & Wu, F. C., Preparation of high surface area carbons from Corncob with KOH etching plus CO_2 gasification for the adsorption of dyes and phenols from water. Colloids Surf. A: Physicochem. Eng., **279**(1-3), 69-78 (2006).

52. Aygün, A., Yenisoy-Karakaş, S., & Duman, I., Production of granular activated carbon from fruit stones and nutshells and evaluation of their physical, chemical and adsorption properties. Microporous Mesoporous Mater., **66**(2-3), 189-195 (2003).

53. Ezzati, R., Derivation of pseudo-first-order, pseudo-second-order and modified pseudo-first-order rate equations from Langmuir and Freundlich isotherms for adsorption. Chem. Eng. J, **392**: 123705 (2020).